Int. J. Radiation Oncology Biol. Phys., Vol. ■, No. ■, pp. 1–7, 2011

0360-3016/$ - see front matter

ELSEVIER

doi:10.1016/j.ijrobp.2011.03.023

PHYSICS CONTRIBUTION

MEGAVOLTAGE IMAGE-BASED DYNAMIC MULTILEAF COLLIMATOR TRACKING OF A NITI STENT IN PORCINE LUNGS ON A LINEAR ACCELERATOR

Per R. Poulsen, Ph.D.,* Jesper Carl, Ph.D.,† Jane Nielsen, M.Sc.,† Martin S. Nielsen, M.Sc.,† Jakob B. Thomsen, M.Sc.,† Henrik K. Jensen, M.D.,‡ Benedict Kjærgaard, M.D.,§ Peter R. Zepernick, M.D.,§ Esben Worm, M.Sc.,* Walther Fledelius, Ph.D.,* Byungchul Cho, Ph.D.,‖ Amit Sawant, Ph.D.,¶ Dan Ruan, Ph.D.,# and Paul J. Keall, Ph.D.**††

*Department of Oncology, Aarhus University Hospital, Aarhus, Denmark; †Department of Medical Physics, Aalborg Hospital, University of Aarhus, Aalborg, Denmark; ‡Department of Pulmonary Medicine, Aalborg Hospital, University of Aarhus, Aalborg, Denmark; §Department of Thoracic Surgery, Aalborg Hospital, University of Aarhus, Aalborg, Denmark; ‖Department of Radiation Oncology, Asan Medical Center, University of Ulsan College of Medicine, Seoul, Korea; ¶University of Texas Southwestern Medical Center, Dallas, TX; #Department of Radiation Oncology, University of California–Los Angeles, Los Angeles, CA; **Department of Radiation Oncology, Stanford University, Stanford, CA; and ††Sydney Medical School, University of Sydney, Sydney, New South Wales, Australia

Purpose: To investigate the accuracy and potential limitations of MV image-based dynamic multileaf collimator (DMLC) tracking in a porcine model on a linear accelerator.

Methods and Materials: A thermo-expandable NiTi stent designed for kilovoltage (kV) X-ray visualization of lung lesions was inserted into the bronchia of three anaesthetized Göttingen minipigs. A four-dimensional computed tomography scan was used for planning a five-field conformal treatment with circular multileaf collimator (MLC) apertures. A 22.5 Gy single fraction treatment was delivered to the pigs. The peak-to-peak stent motion was 3 to 8 mm, with breathing periods of 1.2 to 4 s. Before treatment, X-ray images were used for image-guided setup based on the stent. During treatment delivery, continuous megavoltage (MV) portal images were acquired at 7.5 Hz. The stent was segmented in the images and used for continuous adaptation of the MLC aperture. Offline, the tracking error in beam's eye view of the treatment beam was calculated for each MV image as the difference between the MLC aperture center and the segmented stent position. The standard deviations of the systematic error Σ and the random error σ were determined and compared with the would-be errors for a nontracking treatment with pretreatment image-guided setup.

Results: Reliable stent segmentation was obtained for 11 of 15 fields. Segmentation failures occurred when image contrast was dominated by overlapping anatomical structures (ribs, diaphragm) rather than by the stent, which was designed for kV rather than MV X-ray visibility. For the 11 fields with reliable segmentation, Σ was 0.5 mm/0.4 mm in the two imager directions, whereas σ was 0.5 mm/1.1 mm. Without tracking, Σ and σ would have been 1.7 mm/1.4 mm and 0.8 mm/1.4 mm, respectively.

Conclusion: For the first time, *in vivo* DMLC tracking has been demonstrated on a linear accelerator showing the potential for improved targeting accuracy. The study mimicked the envisioned patient workflow of future patient treatments. Clinical implementation of MV image-based tracking would require markers designed for MV visibility. © **2011 Elsevier Inc.**

Image-guided radiotherapy, Intrafraction motion, Tumor tracking, Dynamic MLC tracking.

INTRODUCTION

Most tumors move during radiotherapy treatment delivery (1–3). This intrafraction motion is usually accounted for by treating a static volume that includes both the tumor and its anticipated motion with a high probability (4). Although this approach often causes increased healthy tissue irradiation with potentially enhanced side effects, part of the tumor may still move outside of the predesigned target

Reprint requests to: Per R. Poulsen, Ph.D., Aarhus University Hospital, Department of Oncology, Nr Brogade 44, 8000 Aarhus C, Denmark. Tel: +45 8949 2651; Fax: +45 8949 4522; E-mail: perpolse@rm.dk

This work was supported by US National Institutes of Health/National Cancer Institute Grant R01 CA93626, Varian Medical Systems (Palo Alto, CA), Pnn Medical (Denmark), The Danish Cancer Society, and CIRRO—The Lundbeck Foundation Center for Interventional Research in Radiation Oncology, and The Danish Council for Strategic Research.

Conflict of interest: This work was partially supported by Varian Medical Systems (Palo Alto, CA) and by Pnn Medical (Denmark).
Acknowledgments—The authors gratefully thank Herbert Cattell, Varian Medical Systems, for substantial development of the DMLC tracking program, and Julie Baz, the University of Sydney, for reviewing this manuscript.

Received Dec 22, 2010. Accepted for publication March 21, 2011.

volume, leading to lower tumor doses than prescribed. An alternative to the static target volume approach is tumor tracking, in which real-time tumor position monitoring is used for repeated realignment of the treatment beam to the tumor position.

To date, tumor tracking has been implemented clinically only for the robotic Cyberknife system (Accuray Inc., Sunnyvale, CA) (5, 6). However, tracking with conventional gantry-mounted linear accelerators has been the subject of several phantom studies that used either continuous couch position corrections (7) or dynamic multileaf collimator (DMLC) tracking (8, 9) for target motion compensation. In this study, the first demonstration of *in vivo* DMLC tracking in a mammal is presented, and the accuracy and potential limitations of the tracking is investigated. The equipment and workflow in the study is analogous to that of current patient stereotactic body radiotherapy treatments.

METHODS AND MATERIALS

MV image-based DMLC tracking

Three Göttingen minipigs were included in the study, which was carried out at Aalborg Hospital, Aarhus University Hospital, Denmark. The study was approved by The Animal Ethics Council under the Danish Justice Department (journal no. 2008/561-1473). A thermo-expandable NiTi stent (7-mm length, 3.5- to 6-mm diameter; Pnn Medical, Denmark) designed for kilovoltage (kV) X-ray visualization of lung lesions was inserted into the bronchia of the pigs under bronchoscope guidance (10) (Fig. 1). Immediately after the lung stent insertion, a planning four-dimensional computed tomography (CT) scan was acquired while the pigs were intubated and ventilated using a respirator. Anesthesia was maintained during these procedures. The mid-expiration CT phase was used for planning of a 6 MV five-field conformal treatment with 6 cm circular multileaf collimator (MLC) apertures and the isocenter located at the stent. For all fields, the collimator rotation was 90°, resulting in MLC leaf motion parallel to the cranio-caudal (CC) direction.

Four weeks after stent insertion, the treatment was delivered to the pigs with a Varian Clinac iX linear accelerator equipped with an AS1000 portal imager on an ExactArm, a Millennium MLC, and a prototype DMLC tracking system (Varian Medical Systems, Palo Alto, CA). Each pig received a single fraction with 22.5 Gy to the isocenter delivered with a dose rate of 600 MU/min. The pigs were anaesthetized before the treatment and kept anaesthetized until after the treatment, when they were sacrificed. Two pigs breathed freely during treatment and one pig was ventilated by the respirator. For the pretreatment alignment, two sequential X-ray images were acquired with an ExacTrac X-ray system (BrainLAB AG, Feldkirchen, Germany) and used for image-guided couch correction based on the stent location. If the stent was captured in different positions in the X-ray images because of respiratory motion, the resulting error in the stent registration with the planning CT scan was distributed evenly among the two X-ray images. Before each field delivery, 10 to 20 continuous megavoltage (MV) images were acquired at 7.5 Hz and stored on the MV imager work station. The exposure dose was 1.33 MU and the exposure time was 133 ms for each image. The source–imager distance for the MV imager was 150 cm, resulting in a pixel side length of 0.261 mm when scaled to isocenter distance. In an in-house marker segmentation program (11), a rectangular area with 6- to 13-mm side lengths that encompassed the stent was manually selected in the first prefield MV image and used as a template for testing template based segmentation in the prefield images that followed. If the segmentation succeeded, the field delivery was ready to start. If the segmentation failed in one or more images, an alternative template was selected among the prefield MV images, and its use for template based segmentation was tested in the other images.

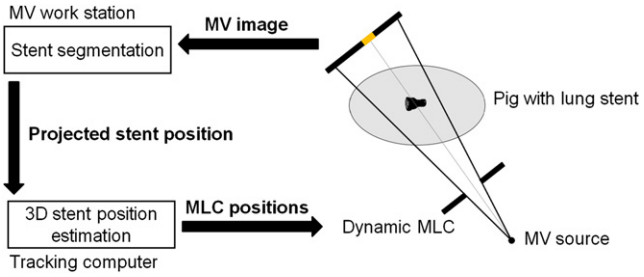

Fig. 2. Megavoltage (MV) image-based dynamic multileaf collimator tracking feedback loop.

During field delivery, continuous MV images were acquired at 7.5 Hz and used for DMLC tracking as illustrated in Fig. 2. When a new MV image was stored on the MV work station, the segmentation program identified the stent in the image by using the prefield selected template and sent the projected stent position to a tracking program on a dedicated tracking computer. The tracking program first estimated the three-dimensional (3D) stent position from the two-dimensional (2D) projected position by assuming that the stent was located in a plane at isocenter distance (100 cm) from the linac MV source. Then a kernel density estimation

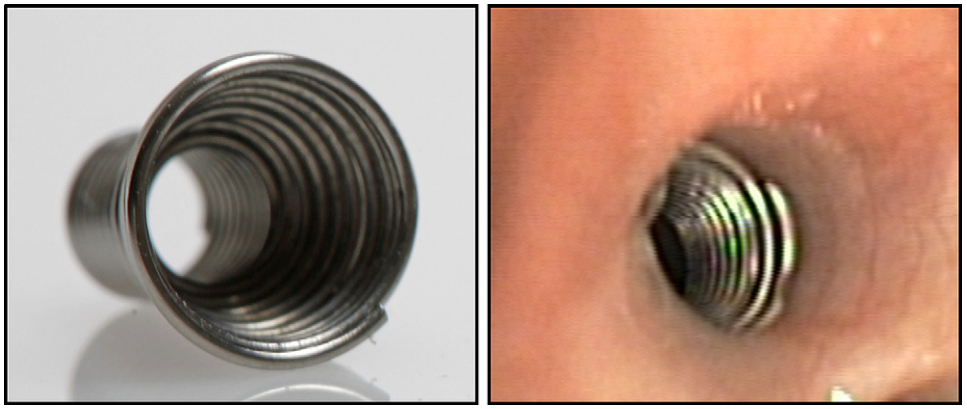

Fig. 1. (Left) Photograph of NiTi stent before insertion. (Right) Bronchoscope image of inserted NiTi stent.

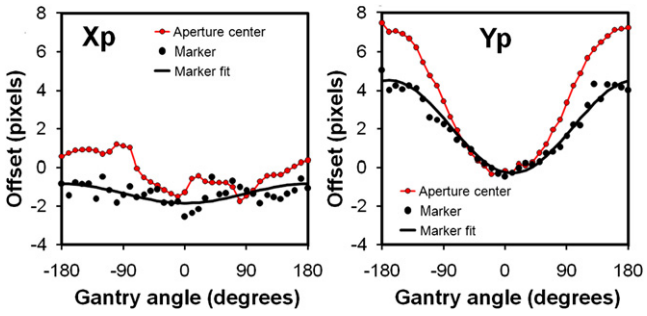

Fig. 3. Imager calibration data. Projected position (relative to the megavoltage imager center) of a marker located in the isocenter shown as a function of gantry angle (black circles). Sinusoidal fit used for imager offset correction (black curve). Projected center position of a non-shifted 6 cm circular multileaf collimator (MLC) aperture (red). Data are shown perpendicular (Xp) and parallel (Yp) to the cranio-caudal axis. One pixel is 0.261 mm.

based prediction algorithm (12) was applied to account for the tracking system latency of 400 ms (13). Finally, the MLC aperture was adjusted to the resulting 3D stent position estimation (14). The prediction was not applied in the first 8 s of each field delivery because a training data set for the prediction algorithm needed to be established first. The training data set was either all MV images acquired for the field (in the period from 8–20 seconds) or a continuously moving window of the MV images acquired in the most recent 20 s. The mean field delivery duration was 59 s (range, 51–71 s) with a mean of 590 monitor units (MU) per field (range, 506–708 MU). The treatment duration from acquisition of the first pretreatment MV image to treatment completion ranged from 30 to 35 minutes for the three treatments.

After the treatments, the tracking error in beam's eye view of the treatment beam was calculated for each intrafield MV image as the difference between the segmented stent position and the MLC aperture center position. For comparison, the error without tracking was calculated as the difference between the intrafield stent positions and the MLC aperture center position after pretreatment alignment (*i.e.,* the MLC aperture in the prefield images before start of the tracking). For each individual field, the root-mean-square (RMS), the mean, and the standard deviation (SD) of the errors were calculated with and without tracking in both directions of the MV imager. The group mean error M was calculated as the mean of the individual mean errors. The group systematic error Σ was calculated as the SD of the individual mean errors. The group random error σ was calculated as the root-mean-square of the individual SD errors. Fields without successful segmentation in the prefield images were not included in this analysis.

Imager calibration and corrections for gantry sag and irreproducible imager positioning

Before the tracking experiments, an MV image of a static marker positioned in the accelerator isocenter was acquired for every 10° gantry angle for imager position calibration (11). The black circles in Fig. 3 show the offset of the marker projection relative to the MV imager center pixel. This gantry dependent offset was a result of gantry sag, imager sag, and imager misalignment. In the tracking experiments, a sinusoidal fit to the offset (black curve in Fig. 3) was used to correct for the offset (11). As a result, the 3D position of a target in the isocenter would be estimated correctly except for inaccuracies in the segmentation, the sinusoidal offset approximation, and the reproducibility of the MV imager positioning.

Nevertheless, gantry sag still contributed to a gantry dependent tracking error. The red curves in Fig. 3 show the projection of the nonshifted (*i.e.,* nontracking) MLC aperture center in the MV calibration images. Although the MLC aperture was reasonably aligned with the isocenter marker for anterior fields (gantry 0), it was approximately 0.8 mm (3 pixels) cranial of the isocenter marker for posterior fields (gantry $\pm$ 180), as seen in the right graph of Fig. 3. This effect of gantry sag could easily be accounted for during DMLC tracking in general by adding a gantry-dependent offset (equal to the difference between the black and the red curves in Fig. 3) to the MLC position. Furthermore, specifically for MV image-based DMLC tracking, it would be straightforward also to correct for irreproducible MV imager positioning because the current MV imager position relative to the imager position at calibration can be determined by comparing the projected (nonshifted) MLC position in the prefield images with the projected MLC position in the calibration images (*i.e.,* the red curves in Fig. 3). Although these corrections for gantry sag and nonreproducible positioning of the MV imager were not made in the current experiments, their effect was quantified in this study by calculating the would-be tracking error if the corrections had been made.

RESULTS

Figure 4 shows a kV X-ray image pair used for the stent based couch correction before treatment start. All stents were clearly visible in the kV setup images. Figure 5 shows three examples of MV images used for the tracking. In general, the stent visibility was markedly reduced in the MV images as compared with the kV images. Reliable MV image-based tracking was obtained for 11 of the 15 fields. Results will be reported for these 11 fields only. The stent segmentation failures occurred when the image contrast was dominated by overlapping anatomical structures, *e.g.,* bones or diaphragm, rather than by the stent. It should be noted that the current version of the stent was specifically designed for kV imaging, *i.e.,* for reduced kV CT artifacts at the cost of reduced contrast in MV images.

Figure 6 shows the position of the stent and the MLC aperture center as recorded in portal images for the first treatment field for each pig. The positions are shown relative to the non-shifted MLC aperture position, which is known from the prefield images. Without DMLC tracking the MLC aperture would remain at the non-shifted zero position throughout the field delivery. Pigs 1 and 2 (Figs. 6a, 6b) were breathing freely and Pig 3 (Fig. 6c) was ventilated with a respirator. For Pig 1 and Pig 2, the stent motion was predominantly in the CC direction with a peak-to-peak motion of 3 mm and 6 mm, respectively, and breathing periods of 2 s and 1.2 s, respectively. For Pig 3, the peak-to-peak motion was approximately 2 mm (left–right), 4 mm (CC), and 6 mm (anterior-posterior) as estimated from the 5 treatment field directions, and the breathing period was 4 s. For this pig, the stent was located close to the heart resulting in the superimposed high frequency cardiac induced motion in Fig. 6c.

As seen in Fig. 6, the prediction started 8 s into the field delivery after acquisition of the first sixty MV images. In the first period without prediction, the MLC motion quite accurately mimicked the stent motion, but with a delay of 400

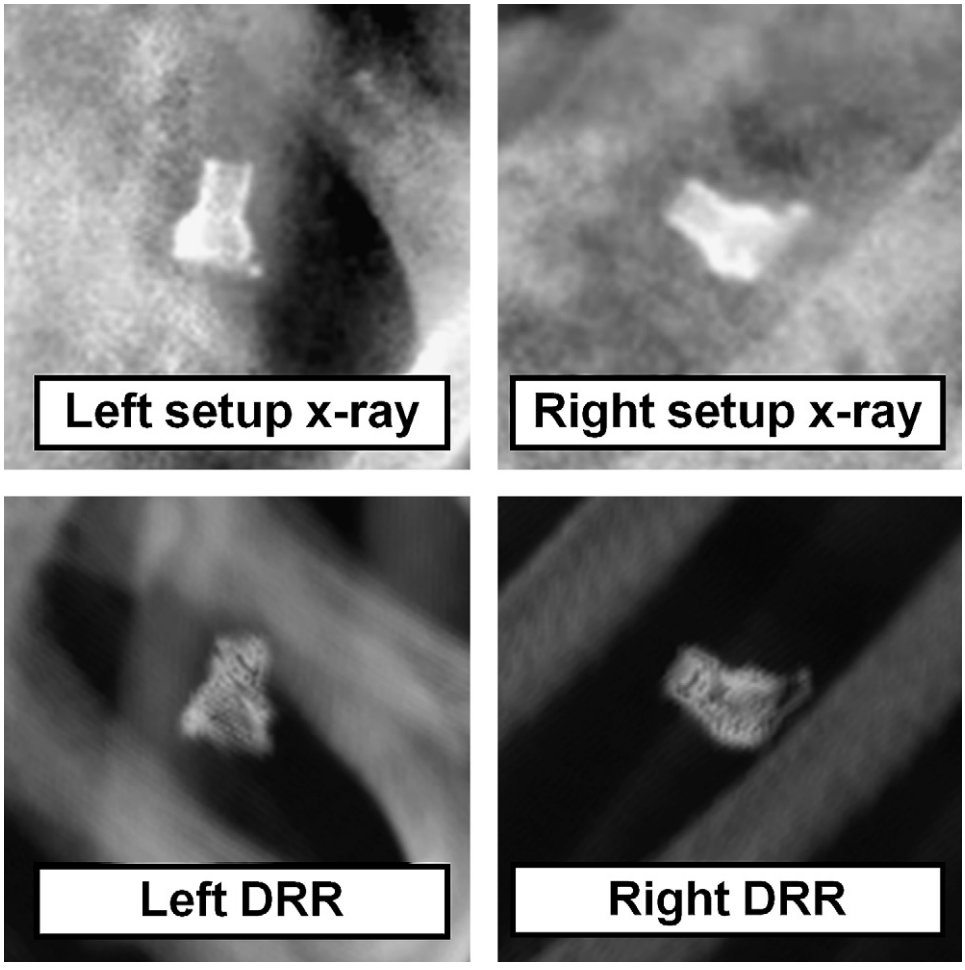

Fig. 4. Pair of sequential kilovoltage X-ray images used for image guided pretreatment localization of a NiTi stent in the lung of a pig (top row) and the corresponding digitally reconstructed radiographs (DRRs) from the planning computed tomography scan (bottom row).

ms as seen in the figure. When prediction started, the MLC motion came into phase with the stent motion, but prediction errors also caused the MLC motion to mimic the stent motion less accurately. The difference between the stent position and the MLC center position in Fig. 6 is the tracking error and the stent position relative to zero is the would-be

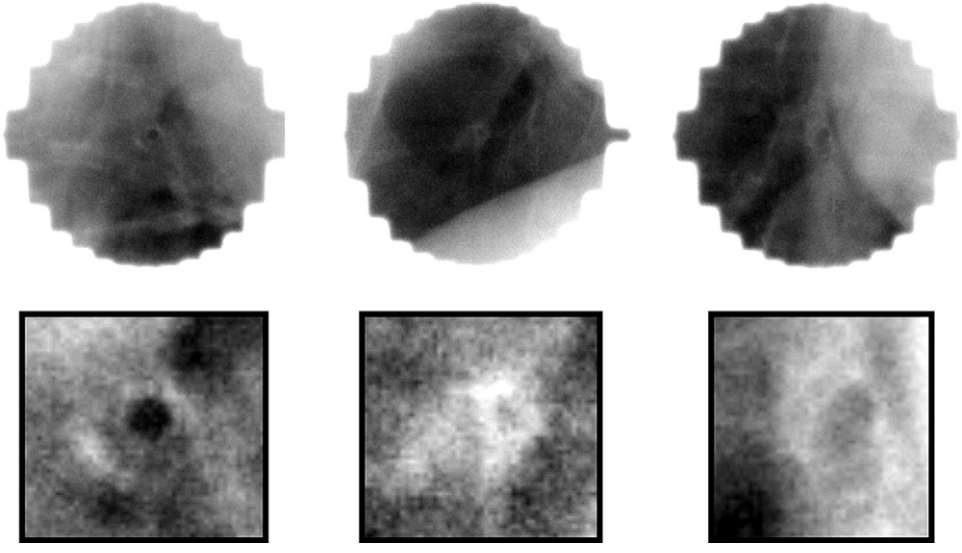

Fig. 5. (Top row) Three examples of megavoltage (MV) images used for dynamic multileaf collimator tracking. (Bottom row) Fourfold magnification of the middle part of the MV images, where the stent is located.

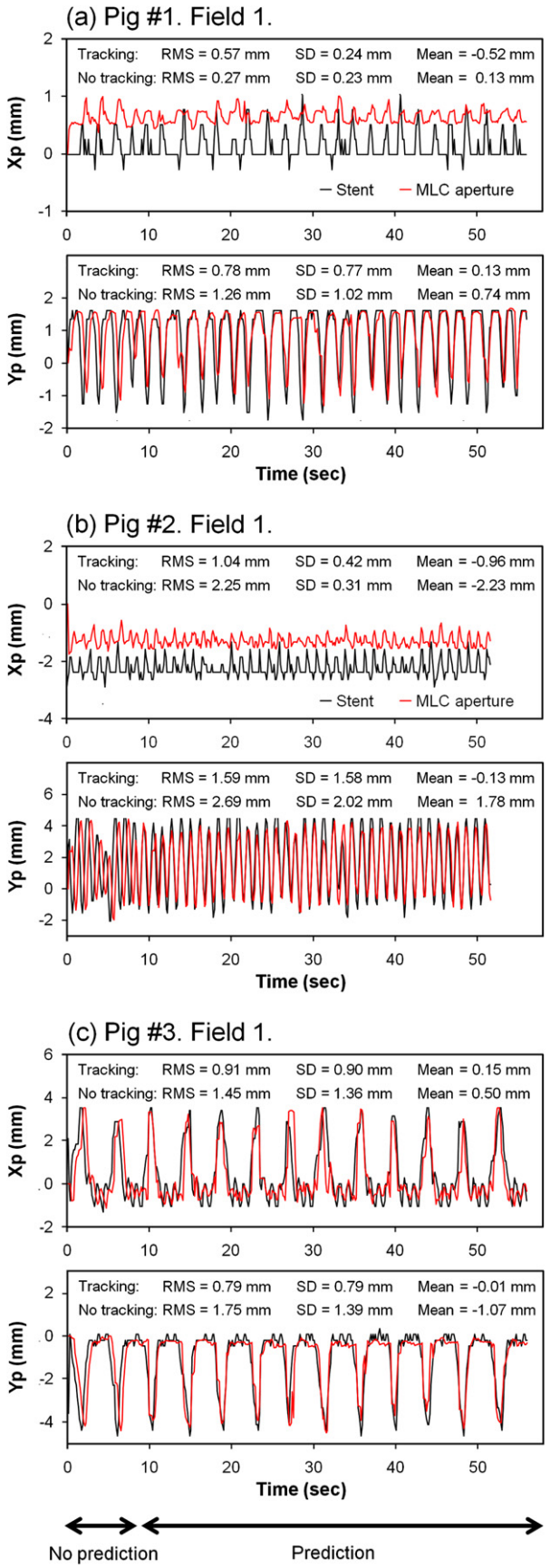

Fig. 6. Motion of stent (black) and multileaf collimator (MLC) aperture center (red) during dynamic multileaf collimator (DMLC) tracking for the first field for each pig as recorded by the megavoltage imager perpendicular (Xp) and parallel (Yp) to the craniocaudal axis. Numbers denote the root-mean-square, the standard deviation, and the mean of the tracking error as well as the would-be errors without tracking.

error without tracking. The RMS value, SD, and mean of these errors are indicated for the fields in Fig. 6. Figure7 shows four different calculations of the RMS error for each treatment field with reliable stent segmentation. Comparing the black columns (no tracking) with the red columns (tracking) shows that DMLC tracking substantially reduced the RMS error for most fields. However, exceptions occurred, for example, in the Xp direction in the first field for Pig 1 (Fig. 6a and Fig. 7, upper left). The green columns in Fig. 7 show that exclusion of the first 60 images where prediction was applied had only a small effect on the RMS tracking error except for Pig 2 in the Yp direction. Because of the fast breathing for this pig, the tracking latency of 400 ms was comparable to half of a breathing cycle (600 ms), which resulted in substantial tracking errors when the latency was not compensated by prediction (Fig. 6b).

As explained in the Methods and Materials section, the expected tracking error caused by gantry sag can be estimated for each field from the imager calibration curves (Fig. 3), whereas the expected error caused by irreproducible MV imager positioning can be estimated by comparing the projected MLC position in the prefield images with the calibration curves. Figure 8 is a scatter plot showing the sum of these error estimations vs. the actual experimental mean tracking error. The estimated errors corresponded reasonably to the actual mean tracking errors for all fields; the largest difference being 0.3 mm. As a result, a large part of the mean tracking error could be corrected for by shifting the MLC aperture to counteract for the estimated error. The blue columns in Fig. 7 show that application of this correction would lead to a substantial reduction in tracking errors.

Table 1 summarizes the mean RMS errors for the four scenarios in Fig. 7, along with the population mean error M and the standard deviations of the systemic error Σ and the random error σ. The table also shows $2.5\Sigma + 0.7\sigma$, which is often used to quantify the setup margin needed to ensure a minimum target dose of 95% with 90% probability (15). As shown in the table, this margin is largely reduced by the tracking. However, the margin formalism assumes that the overall population mean M is negligible compared with Σ and σ. Because this requirement is not fulfilled in current tracking experiments (Fig. 8, Table 1), $2.5\Sigma + 0.7\sigma$ underestimates the necessary setup margins for these experiments. However, if the suggested corrections for gantry sag and irreproducible imager positioning had been applied, M would be negligible and large setup margin reductions would be possible (Table 1, last row).

DISCUSSION

The experiments in this study represent the first demonstration of *in vivo* DMLC tracking for a mammal. As the

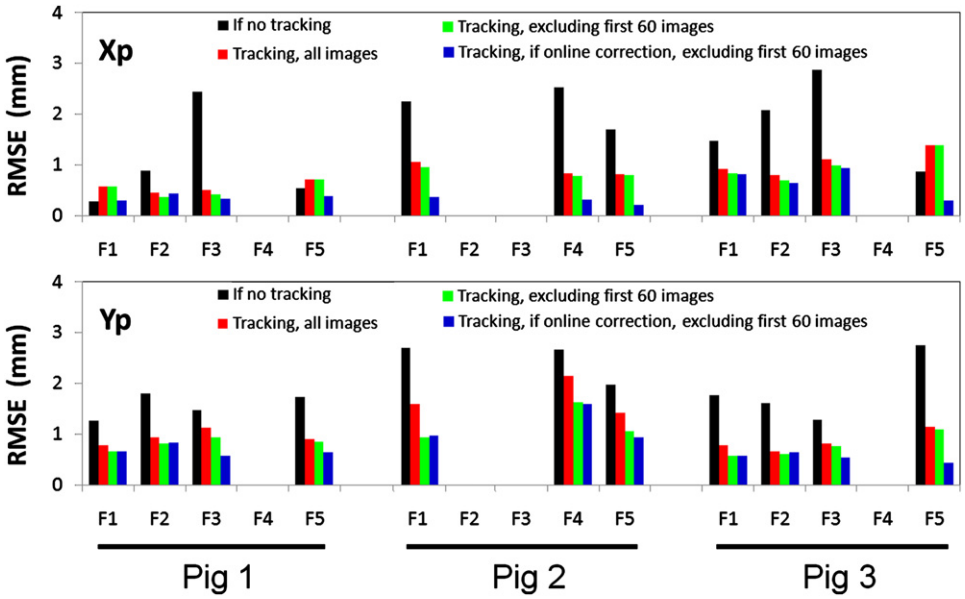

Fig. 7. Root-mean-square multileaf collimator (MLC) position error for the 11 fields with reliable stent segmentation in case of no tracking (black); as observed during dynamic multileaf collimator (DMLC) tracking (red); with tracking when excluding the first sixty Megavoltage (MV) images with no prediction (green); and with tracking if correction for gantry sag and non-reproducible MV imager positioning had been made (blue). Xp and Yp denote the MV imager directions perpendicular and parallel to the cranio-caudal axis, respectively.

equipment and workflow were analogous to that of patient stereotactic body radiotherapy treatments, the demonstration is an important step toward clinical implementation of DMLC tracking. Reliable tracking was obtained for 11 of 15 fields showing substantial accuracy improvements compared with on-line image-guided radiotherapy without tracking. By highlighting main advantages and disadvantages of MV image-based tracking, this study can serve as a guide for a safe clinical introduction of the tracking method. The main advantages of MV image-based DMLC tracking are the avoidance of additional imaging dose to the patient and the direct visualization of the target (surrogate) position within the field shape formed by the MLC leaves. Although not done in the current study, the dose for the prefield images could be subtracted from the intrafield dose to obtain dose-neutral imaging for tracking. Furthermore, the imaging of both target and MLC in the MV images can be used for considerable systematic error reductions by compensating for irreproducible imager positioning (Table 1, last row).

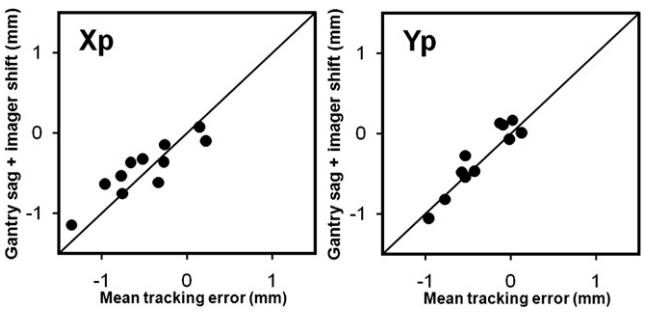

Fig. 8. Experimental mean tracking error vs. the expected error stemming from gantry sag and irreproducible imager positioning for the 11 fields with reliable stent segmentation perpendicular (Xp) and parallel (Yp) to the cranio-caudal axis. A line with unity slope is shown for reference.

The main disadvantages of MV image-based tracking are related to the MV image quality and the tight coupling between the MV image-based target localization and the treatment delivery. First, although the setup kV images showed very good contrast for all stents, MV contrast limitations resulted in unreliable stent segmentation, and thus failed tracking, in four of the 15 fields in this study. Therefore, markers designed for better MV visibility would be needed for clinical implementation of MV image-based tracking. Second, the temporal limitation of MV image-based localization to the treatment delivery time hindered the use of prediction until a sufficient training data set had been collected (8 s into the field delivery in this study). The temporal limitation of MV imaging also hampers MV image-based gating because the MV images cannot be used to determine when to turn on the beam after a beam-off period. Third, the spatial limitation of the MV field-of-view to the MLC aperture hinders straightforward integration with intensity modulated treatments (IMRT and IMAT) because the target may be blocked by the MLC leaves. Although strategies to circumvent this limitation have been proposed (16), MV image-based DMLC tracking may be restricted to conformal treatments and cases in which the entire marker is located well within the planning target volume.

A further limitation of the MV image-based tracking in the current study is the lack of a full 3D target position estimation. The tracking was effectively 2D tracking in the MV resolved plane as the target was always assumed to be located at isocenter distance from the MV source. Usually this 2D in-plane tracking will only deviate negligibly from

Table 1. Summary of tracking errors observed in megavoltage (MV) images perpendicular (Xp) and parallel (Yp) to the cranio–caudal axis

	Mean RMS error		M		Σ		σ		$2.5\Sigma + 0.7\sigma$	
Motion compensation	Xp	Yp	Xp	Yp	Xp	Yp	Xp	Yp	Xp	Yp
Without tracking	1.6	1.9	0.1	0.3	1.7	1.4	0.8	1.4	4.9	4.5
Tracking, all MV images	0.8	1.1	−0.5	−0.4	0.5	0.4	0.5	1.1	1.5	1.6
Tracking, excluding prediction training	0.8	0.9	−0.5	−0.4	0.5	0.4	0.5	0.8	1.5	1.5
Tracking, gantry sag and imager position correction	0.5	0.8	−0.06	−0.05	0.2	0.2	0.5	0.8	0.9	1.0

Abbreviations: M = group mean error; Σ = group systematic error; σ = group random error.
All units are given in millimeters.

full 3D tracking, where in-depth motion along the treatment beam axis is tracked by magnification or de-magnification of the MLC aperture (14). However, the simplification to 2D in-plane tracking means that also the target position prediction (and the corresponding training data set collection) was performed in the resolved plane of the MV imager only. Consequently, a new prediction training data set had to be established for each beam direction. This substantially complicates the use of prediction for 2D in-plane tracking in arc therapy. However, a consistent 3D prediction training data set in a fixed coordinate system could be obtained by estimating the full 3D target trajectory during the rotation (17).

Despite the limitations, this study suggests that the following conservative strategy could lead to safe clinical implementation of MV image-based DMLC tracking. After implantation of markers with good MV contrast, a conformal treatment plan with standard motion margins (15) is produced. Continuous MV images are acquired during field delivery, but no tracking is performed during the first part of the field delivery. If the segmentation is reliable, the DMLC tracking is started when sufficient images for prediction training are acquired. In case of any uncertainty, the tracking is stopped, the MLC leaves are moved back to their preplanned positions, and the remaining part of the treatment field is delivered as a standard nontracking treatment. As this conservative scenario does not involve margin reductions, the aim would not be a smaller treated volume; instead, the aim would be an improved tumor dose for the 10% of treatments in which standard motion margins fail to ensure a minimum CTV dose of 95% (15). If introduced carefully, this gain in delivery robustness should come at no cost in terms of additional imaging dose or risks to the patient.

CONCLUSION

For the first time, *in vivo* DMLC tracking has been demonstrated showing the potential for improved targeting accuracy. Clinical implementation of MV-based tracking would require markers designed for MV visibility.

REFERENCES

1. Langen KM, Jones DT. Organ motion and its management. *Int J Radiat Oncol Biol Phys* 2001;50:265–278.
2. Keall PJ, Mageras GS, Balter JM, *et al*. The management of respiratory motion in radiation oncology report of AAPM Task Group 76. *Med Phys* 2006;33:3874–3900.
3. Shirato H, Seppenwoolde Y, Kitamura K, *et al*. Intrafractional tumor motion: Lung and liver. *Semin Radiat Oncol* 2004;14:10–18.
4. ICRU Report 62: Prescribing, recording and reporting photon beam therapy (supplement to ICRU Report 50). Bethesda: International Commission on Radiation Units and Measurements; 1999.
5. Schweikard A, Shiomi H, Adler J. Respiration tracking in radiosurgery. *Med Phys* 2004;31:2738–2741.
6. Murphy MJ. Tracking moving organs in real time. *Semin Radiat Oncol* 2004;14:91–100.
7. D'Souza WD, Naqvi SA, Yu CX. Real-time intra-fraction-motion tracking using the treatment couch: A feasibility study. *Phys Med Biol* 2005;50:4021–4033.
8. Keall PJ, Kini VR, Vedam SS, *et al*. Motion adaptive x-ray therapy: A feasibility study. *Phys Med Biol* 2001;46:1–10.
9. Neicu T, Shirato H, Seppenwoolde Y, *et al*. Synchronized moving aperture radiation therapy (SMART): Average tumour trajectory for lung patients. *Phys Med Biol* 2003;48:587–598.
10. Carl J, Jensen HK, Nielsen J, *et al*. A new fiducial marker for gated radiotherapy in the lung: A feasibility study of bronchoscopy based insertion and removal in Göttingen mini-pig. *Scandinavian J Lab Anim Sci* (in press).
11. Cho B, Poulsen PR, Sloutsky A, *et al*. First demonstration of combined kV/MV image-guided real-time DMLC target tracking. *Int J Radiat Oncol Biol Phys* 2009;74:859–867.
12. Ruan D. Kernel density estimation-based real-time prediction for respiratory motion. *Phys Med Biol* 2010;55:1311–1326.
13. Poulsen PR, Cho B, Sawant A, *et al*. Detailed analysis of latencies in image-based dynamic MLC tracking. *Med Phys* 2010; 37:4998–5005.
14. Sawant A, Venkat R, Srivastava V, *et al*. Management of three-dimensional intrafraction motion through real-time DMLC tracking. *Med Phys* 2008;35:2050–2061.
15. van Herk M, Remeijer P, Rasch C, *et al*. The probability of correct target dosage: Dose-population histograms for deriving treatment margins in radiotherapy. *Int J Radiat Oncol Biol Phys* 2000;47:1121–1135.
16. Ma Y, Lee L, Keshet O, *et al*. Four-dimensional inverse treatment planning with inclusion of implanted fiducials in IMRT segmented fields. *Med Phys* 2009;36:2215–2221.
17. Poulsen PR, Cho B, Ruan D, *et al*. Dynamic multileaf collimator tracking of respiratory target motion based on a single kilovoltage imager during arc radiotherapy. *Int J Radiat Oncol Biol Phys* 2010;77:600–607.